ACS OMEGA

Open Access

http://pubs.acs.org/journal/acsodf

Article

Total Reflection X-ray Fluorescence Spectrometric Analysis of Ten Lanthanides at the Ultratrace Level Having a High Degree of Overlap in the Emission Lines

Kaushik Sanyal, Abhijit Saha,* Arnab Sarkar,* Sadhan Bijoy Deb, Rajesh V. Pai, and Manoj Kumar Saxena

Cite This: *ACS Omega* 2023, 8, 41402−41410

Read Online

ACCESS | Metrics & More | Article Recommendations | Supporting Information

ABSTRACT: The extensive use of lanthanide elements in the medical, electrical, agricultural, and nuclear fields has increased their contamination in the environment. The detrimental effect of lanthanides on human health can be reduced or eliminated by their fast determination in the concerned specimen. For this purpose, an offline conjugation of the cloud point extraction (CPE) process with total reflection X-ray fluorescence (TXRF) spectrometry was done. This process was found to provide simple, quick, and precise simultaneous determination of ten lanthanides whose emission lines have a high degree of overlap at the ultratrace level. *N*,*N*,*N*′,*N*′-tetra-octyl-diglycolamide in triton X-114 micelles was found to offer a selective CPE of all of the lanthanides in the presence of higher concentrations of naturally abundant cations and anions. A multivariate partial least-squares regression (PLSR) calibration approach was preferred due to the complex overlapped spectra of L lines of the lanthanides. Ten lanthanides, viz., La, Nd, Sm, Eu, Gd, Tb, Dy, Ho, Tm, and Lu, were simultaneously determined by this method, having concentrations in the range from 10 to 5 × 10^3 μg L^{-1}. The proposed method was validated by analyzing three certified reference materials (CRMs), viz., NASS-7 seawater, SRLS-6 river water, and NIST 1640a natural water, via standard addition with the relative standard deviations of ≤10%.

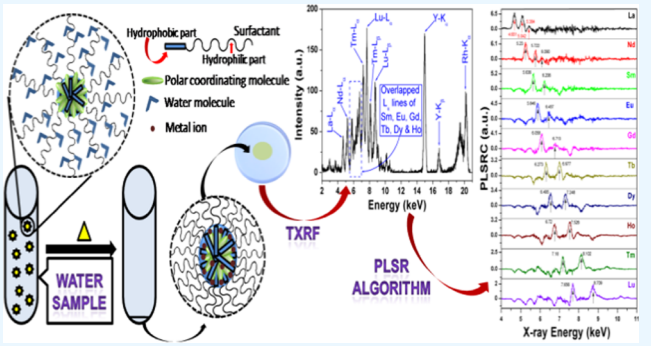

INTRODUCTION

The lanthanide series comprises a total of 15 elements (lanthanum to lutetium). Among them, 14 elements are commonly available in nature, except *Pm*. Lanthanide elements find wide applications in microelectronics, optics, medicine, materials science, and nuclear reactors.[1,2] Some of the lanthanides are also used in fertilizers.[3] Due to their versatile usage, lanthanides are considered to be the most critical elements for clean energy production and high-tech manufacturing.[4] The ever-increasing applications of lanthanides in diverse fields result in anthropogenic emissions of these elements in different environmental samples like soil, water etc. Recent studies have shown that the concentrations of lanthanides are increasing in tap water, surface water, groundwater, seawater, soil, and plants.[5,6] Some investigations have shown that increased concentrations of lanthanides in environmental samples may cause potential health hazards to humans and animals.[7] Excess intake of lanthanides can cause damage to the liver, kidney, and heart.[8,9] Due to similar cationic radii of trivalent La^{3+} and Gd^{3+} to Ca^{2+}, they can block calcium channels in human cells.[10,11] The maximum permissible limit of lanthanides in drinking water is in the range of 7.1−22.1 μg L^{-1}.[12] Consequently, it is important to determine lanthanide concentrations in the environmental samples. As lanthanides are present at ultratrace levels (much less than 1 mg L^{-1}) in environmental samples, it is necessary to develop a highly sensitive analytical methodology. Total reflection X-ray fluorescence (TXRF) is a high-sensitivity variant of the X-ray fluorescence (XRF) method.[13] This analytical technique has several advantages, such as the requirement of a very small sample volume, simple instrumentation, low maintenance cost, multielemental analytical capability, high sensitivity, etc. It can be used to analyze elements ranging from carbon to uranium.[14] It is already a well-established technique for the analysis of different types of environmental samples.[15,16] However, there are several challenges in the case of analyzing lanthanides by TXRF. The first one is low fluorescent yields of lanthanide L lines,

Received: July 17, 2023
Revised: September 5, 2023
Accepted: October 9, 2023
Published: October 24, 2023

which limit their determination at ultratrace levels using this technique. The second problem is severe spectral interference among the L lines of lanthanides, which limits their simultaneous determination in environmental samples. There are limited literature reports on the simultaneous analysis of lanthanides using the TXRF/XRF technique, and none of the work has tackled both of these problems together.[4,17,18] The first problem of low fluorescent yields can be taken care of by using a preconcentration methodology. Various preconcentration methodologies are reported in the literature, like solid-phase extraction (SPE), cloud point extraction (CPE), dispersive liquid−liquid microextraction (DLLME), etc.[4,19−21] Among all of these preconcentration techniques, only CPE generates microliter (μL) volumes of the analyte phase, which is more than sufficient for direct TXRF/XRF measurements. Recently, the CPE technique has emerged as a promising, simple, and environmentally friendly technique for the preconcentration of various elements.[20−26] CPE is basically a single-phase liquid−liquid microextraction process where the dispersed micelle phase separates the metal ion from the aqueous phase to the temperature-driven surfactant-rich phase (SRP) of a few microliters.[20−26] The use of selective ligands and the optimization of parameters are prerequisite to achieve high precencentration factor (PF) and percentage recovery (% Rec) for any metal ion by CPE.[26] There are only a few reports where the CPE technique has been used in combination with TXRF.[20,22] However, there is no single report in which CPE is used in combination with TXRF for the analysis of lanthanides. Most of the lanthanides are expected to be simultaneously extracted by CPE because the majority of these elements exhibit an oxidation state of +3 in the solution phase.

In this work, we have used a micellar dispersion containing *N*,*N*,*N*′,*N*′-tetra-octyl-diglycolamide (TODGA) for the preconcentration of lanthanides present at the ultratrace level in different types of environmental water samples. A total of ten lanthanides, viz., La, Nd, Sm, Eu, Gd, Tb, Dy, Ho, Tm, and Lu, were preconcentrated by CPE and then analyzed by TXRF technique. Generally, analysis of XRF/TXRF spectra has been done using the nonlinear least-squares fitting algorithm.[27] However, this algorithm failed to provide precise and accurate results in this case due to severe overlap of lanthanide L lines. Therefore, in this study, we have used the partial least-squares regression (PLSR) algorithm to deconvolute the complex XRF spectra of ten lanthanides of interest. PLSR analysis establishes a mathematical relation between a matrix with analytical responses and a vector with property of interest.[26,28] This statistical method can provide good results while analyzing samples containing complex matrices.[29] Simultaneous analysis of such a large number of lanthanides at the ultratrace level with overlapping spectral interference has been done for the first time using the TXRF technique. The proposed analytical methodology has been validated by analyzing the recovery of ten lanthanides in three unique certified reference materials (CRMs) via the standard addition method. In the present work, our main aim is to show that it is possible to analyze lanthanides having a very high degree of overlap at the ultratrace level. We have established a state-of-the-art technique where we have combined preconcentration of lanthanides with TXRF followed by the PLSR algorithm. This allows us to analyze lanthanide elements at the ultratrace level even though their X-ray characteristic lines are closer than the resolution of the detector, which is generally used for TXRF/XRF measurements. The details of the study carried out are described in the paper.

2. EXPERIMENTAL SECTION

2.1. Materials and Instruments. Chloroacetyl chloride (98%), di-*n*-octyl amine (97%), acetonitrile (anhydrous, 99.8%), *N*,*N*-dimethylformamide (anhydrous, 99.8%), sodium hydride (dry, 90%), tetrahydrofuran (anhydrous, ≥99.9%, inhibitor-free), methanol (anhydrous, 99.8%), chloroform (anhydrous, ≥99%, containing 0.5−1.0% ethanol as a stabilizer), and sodium acetate (anhydrous, ≥99%) were purchased from Sigma-Aldrich. TODGA was synthesized using the method proposed by Dicholkar et al.[30] Other reagents used were HNO_3 (Merck), sodium hydroxide (NaOH, Merck), potassium nitrate (KNO_3, Alfa Aesar), Triton X-114 (TTX-114, Sigma-Aldrich), and ethyltrimethylammonium bis(trifluoromethylsulfonyl)imideacetonitrile ($[C_2mim][NTf_2]$; 99%, Sigma-Aldrich). Milli-Q water (18MΩ·cm) was used throughout the experiments. Dynamic light scattering (DLS) experiments were performed by using a Malvern 4800 Autosizer employing a 7132 digital correlator, a 15 mW He−Ne laser light source, and an avalanche photodiode (APD) detector.

All of the TXRF measurements were carried out using a low-Z−high-Z TXRF spectrometer called WOBISTRAX made by Atominstitute, Vienna. The instrument has Rh- and Cr-targeted X-ray tubes fitted with Pd/B_4C and Ni/C multilayers, respectively. Both tubes can be easily slid. The measurements were carried out in air. The monochromatic beam of Rh K_α was used to excite the samples. All of the measurements were carried out at a tube voltage of 50 kV and a tube current of 700 μA. Each sample was measured for a live time of 500 s. The details of the instrument can be found in the literature.[31−33] Flat and polished quartz sample supports with 30 mm diameter and 3 mm thickness were used to deposit samples. The analysis of the TXRF data was carried out by an in-house written PLSR algorithm program in LabVIEW (LabVIEW2012, National Instruments).

2.2. Cloud Point Extraction and TXRF Sample Preparation. A 40 mL aliquot of sample solution was taken in a beaker, and the pH was adjusted to 4 by adding dilute HNO_3 or NH_4OH solution. A 5 mL aliquot of pH 4 buffer and 0.5 g of KNO_3 were added to the solution. Afterward, 2.5 mL of a dispersion of 20 mmol L^{-1} TODGA in 150 mmol L^{-1} TTX-114 and 1 mL of 12.5 mmol L^{-1} $[C_2mim][NTf_2]$ in $CHCl_3$ were added to the above mixture. The solution was stirred at RT (25 ± 1 °C) until $CHCl_3$ was completely evaporated. The solution was then transferred into a conical centrifuge tube, and the volume was made up to 50 mL by adding Milli-Q water. The tube was placed in a rotating mixer for 30 min at RT. After sample equilibration, the tube was placed in a thermostat water bath at 55 ± 1 °C for 1 h. The surfactant-rich phase (SRP) settled down at the bottom, and complete phase separation was done by centrifugation at 2000 rpm for 10 min. The bulk aqueous phase was then pipetted out. A 10 μL volume from the 200 μL SRP was drop-cast on a quartz sample support and then placed in a Muffle furnace at 650 °C for 30 min. After 30 min of oxidative pyrolysis, the quartz sample support was taken out, cooled, and then placed in the TXRF instrument for analysis. The whole process is shown as a schematic diagram in Figure S1 (Supporting Information, SI).

https://doi.org/10.1021/acsomega.3c05139
ACS Omega 2023, 8, 41402−41410

2.3. Partial Least-Squares Regression (PLSR) Algorithm. The PLSR method, which is entirely empirical, was used to calibrate the TXRF spectra of the lanthanide mixture. This method does not necessitate any understanding of the elements' basic physical characteristics, such as their X-ray abundance, energy, etc. A calibration set (CS) of 15 standards, viz., $Ln_{CS}1-Ln_{CS}15$, (Table T1 in the SI), was used to construct the calibration curves for the PLSR algorithm. On the other hand, a validation set (VS) of five standards, viz., $Ln_{VS}16-Ln_{VS}20$, was used to confirm the calibration models. Multivariate calibration was obtained progressively, taking into account all of the intensities at each data point (or pixel, in the case of TXRF spectra), using this method. Multivariate calibration has been demonstrated to be accurate even when spectra are only partially resolved, a phenomenon present in the current complex system.[34] This study's PLS algorithm is comparable to those previously discussed.[34−36] A brief description of the PLSR algorithm is given in Supporting Information (SI).

3. RESULTS AND DISCUSSION

3.1. Optimization of CPE Parameters. The extraction parameters of ten lanthanides by TODGA via the CPE process were optimized to obtain maximum percentage recovery (% Rec) and preconcentration factor (PF) values. The concerned equations of the above-mentioned terms are reported elsewhere.[26,37] The cross-optimization procedure was adopted to fix all of the parameters. The optimized parameters are represented in Table T2 (SI). All of the experiments were carried out with a mixture of ten lanthanides ($Ln_{CS}5$) having different individual concentrations. The details of this lanthanide mixture ($Ln_{CS}5$) are given in Table T1 (SI) and were used after dilution by a factor of 200.

3.1.1. Effect of pH on CPE. CPE is extremely sensitive to sample acidity and commonly carried out in the pH range of 1−10.[26,37] High acidity hampers the coacervation of micelles due to the stripping potential of acids. In this work, the recoveries of lanthanides were carried out in the pH range of 1−6, keeping all other parameters constant, as mentioned in Table T2 (SI). The results are listed in Figure 1. The recoveries of all of the lanthanides are found to increase steadily from pH 1 to 3 and then remain constant up to pH 6.

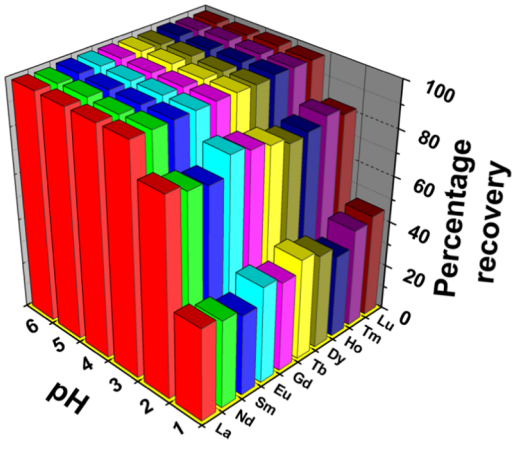

Figure 1. Effect of pH on the recovery (%) of ten lanthanides when all other parameters were kept constant, as mentioned in Table T2 (SI).

The maximum percentage recoveries of all ten lanthanides were found to be >98%. The extraction pattern in the pH range indicates a cation-exchange mechanism for each lanthanide. The observation is similar to the reported liquid−liquid extraction of lanthanides by TODGA from low-acidic samples to room-temperature ionic liquid (RTIL) media.[38]

3.1.2. Effect of TODGA on CPE. TODGA is a well-studied extractant molecule that selectively separates tripositive lanthanides (Ln^{3+}) from both high- and low-acidic solutions.[38,39] At high acidity, TODGA acts as a bidentate ligand and extracts Ln^{3+} ions into the common organic phase, forming the $[Ln(TODGA)_n(NO_3)_3]$ neutral complex, where "n" is 3 for lanthanum and 4 for rest of the lanthanides, as shown in eq 1.[38] On the other hand, TODGA shows tridenticity in low-acidic medium and extracts Ln^{3+} ions as $[Ln(TODGA)_3]^{3+}$ cations into the RTIL medium, as per eq 2. The long octyl chains resulted in easy dispersion of TODGA in the TTX-114 medium. The extraction of lanthanides was carried out in the presence of 0.1−1.25 mmol L^{-1} of TODGA, keeping all other parameters constant, as mentioned in Table T2 (SI). The results are shown in Figure S2 (SI). At and above 0.75 mmol L^{-1} of extractant, the %Rec was found to be >98% for every individual lanthanide. Hence, for safer operations, 1.0 mmol L^{-1} TODGA concentration was chosen.

In a common organic medium

$$Ln^{+3}{}_{aq} + n\text{TODGA}_{org} + 3NO_3^-{}_{aq} \leftrightarrow [Ln(TODGA)_n(NO_3)_3]_{org} (n = 3 \text{ or } 4) \quad (1)$$

In an ionic liquid medium

$$Ln^{+3}{}_{aq} + 3\text{TODGA}_{IL} + 3C_n\text{mim}^+{}_{IL} \leftrightarrow [Ln(TODGA)_3]^{3+}{}_{IL} + 3C_n\text{mim}^+{}_{aq} \quad (2)$$

3.1.3. Effect of TTX-114 on CPE. The nonionic surfactant TTX-114 was chosen because of its low theoretical cloud point temperature (CPT) (28 °C) near RT. In addition, its low CMC of 0.2 mmol L^{-1} would have a minimum toxicological effect on the environment. The concentration of the nonionic surfactant should be sufficient to extract the analytes quantitatively and improve the PFs. The effect of TTX-114 concentration on the recoveries of Ln^{3+} ions was studied in the range of 2.5−12.5 mmol L^{-1}, keeping all other parameters constant, as mentioned in Table T2 (SI). The results of this study are shown in Figure S3 (SI). Quantitative recoveries were observed at and above the 7.5 mmol L^{-1} concentration of TTX-114.

3.1.4. Effect of RTIL on CPE. The cation-exchange extraction mechanism of Ln^{3+} ions at low acidity necessitates the presence of an ion pair in the organic phase. The cationic part of that ion pair must have fair solubility in the aqueous medium to balance the ion exchange, eq 2. In general, the liquid−liquid extraction of Ln^{3+} ions at low acidity uses room-temperature ionic liquids (RTILs) like $[C_2mim][NTf_2]$ in the organic media.[38,39] Hence, we have dispersed the same $[C_2mim][NTf_2]$ along with TODGA in the TTX-114 medium in the concentration range of 0.05−0.40 mmol L^{-1}, keeping all other parameters constant, as mentioned in Table T2 (SI). The results are listed in Figure 2. The recovery improved significantly compared to the one in the absence of RTIL. The

https://doi.org/10.1021/acsomega.3c05139
ACS Omega 2023, 8, 41402−41410

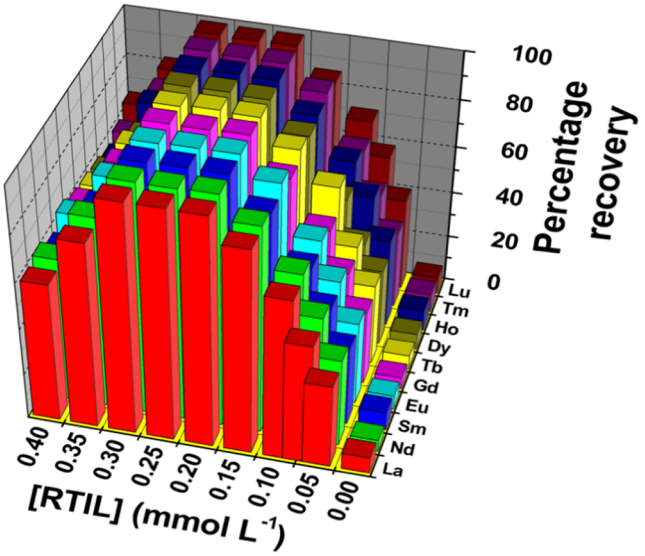

Figure 2. Effect of RTIL concentration on the recovery (%) of ten lanthanides when all other parameters were kept constant, as mentioned in Table T2 (SI).

maximum recoveries of >98% were achieved for all ten lanthanides at and above 0.2 mmol L^{-1} RTIL. A minimum of 0.2 mmol L^{-1} RTIL was required for quantitative recovery of Ln^{3+} ions, and we chose 0.25 mmol L^{-1} RTIL as the optimized value. At a higher RTIL concentration of more than 0.3 mmol L^{-1}, the recovery was found to decrease again. At high RTIL concentrations, the cloud point temperature (CPT) of the system increases due to the higher amount of electrostatic repulsion among the RTIL molecules. This can cause low recoveries of analytes, as per our earlier reports.[26]

3.1.5. Effect of KNO_3 on CPE. Addition of KNO_3 was done to maintain the ionic strength of the micelle medium in the operating pH range. It also acts as a salting-out agent that forces the metal−ligand complex to form inside the micelles. The KNO_3 concentration was varied from 0.1 to 0.5 mol L^{-1}, keeping all other parameters constant, as mentioned in Table T2 (SI). It was observed that the quantitative recoveries of Ln^{3+} ions were obtained over the entire KNO_3 concentration range. Hence, a minimum of 0.1 mol L^{-1} KNO_3 was used throughout the experiments.

3.1.6. Effect of Temperature on CPE. The addition of various additives to the micelle medium is known to alter the CPT significantly.[20−26] Addition of an RTIL ($[C_2mim][NTf_2]$) increases the CPT, whereas the reverse is caused by the addition of an electrolyte (KNO_3).[20−26] Hence, determination of CPT for any new micelle system is a prerequisite, and this was done here by DLS measurements. The measurement was started from 20 °C, and the average micelle size was measured with every 1 °C increase in temperature. The results are represented in Figure S4 (SI). It was found that the size of the micelle increased up to 42 °C and then suddenly started to decrease. This confirmed the CPT of our system to be 42 ± 1 °C. The CPT separates SRP and the bulk aqueous phase, whereas the complete phase separation was done by centrifugation. Phase separation above the CPT of the system was reported to result in a higher PF value compared to the value obtained at CPT. Temperatures above the CPT reduce the phase volume ratio of the SRP more and improve the PF values. Hence, we have carried out the phase separations at temperatures starting from 42 to 65 °C and compared the PF values. The results are shown in Figure S5 (SI). The error bars in Figure S5 represent the spread of PF values of all ten lanthanides and not the standard deviation. The highest PF values were achieved at and above 55 °C.

3.2. TXRF Analysis. Figure 3 shows the TXRF spectrum of one of the aliquot solutions labeled $Ln_{cs}5$ having a mixture of

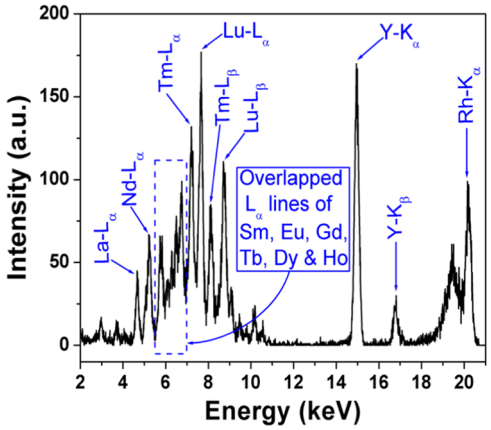

Figure 3. TXRF spectrum of one of the aliquot solutions labeled $Ln_{cs}5$ in Table T1 (SI).

ten lanthanides (La, Nd, Sm, Eu, Gd, Tb, Dy, Ho, Tm, Lu) having different concentrations (see Table T1 in the SI). From Figure 3, it can be seen that all lanthanide elements are clearly visible. However, there is a considerable amount of overlapping among Sm L_α, Eu L_α, Gd L_α, Tb L_α, Dy L_α, and Ho L_α lines in the region of 5.6−6.5 keV, as shown in Figure 3. It is very difficult to separate the peaks in this region. Generally, different software programs like AXIL, PyMcA, or EDXRF 32 are used to fit the TXRF spectra.[40−43] These software use nonlinear least-squares methodology. However, when there is severe spectral interference, like for the L lines of lanthanides, these techniques are no longer good enough. Hence, these programs cannot be applied to generate the individual calibration curves for the ten lanthanides using the same set of solutions ($Ln_{cs}1$−$Ln_{cs}15$). Here, in the AXIL program, we used the Gaussian function to fit the experimental peaks and get the area under each peak. The fitting followed a converging algorithm in an iterative way until the minimum value for χ^2 was found. The efficiency of AXIL fitting is known to be very much dependent on the resolution of the detector. For the present experiment, we have used a silicon drift detector (SDD) from KETEK, and the resolution of the detector at 5.91 keV is 0.136 keV. Table T3 (SI) presents the energies of two main lines (L_3M_5 or L_α and L_2M_4 or L_β) of the ten lanthanide elements. It can be clearly seen that the spectral interference between the L lines is huge and many lines have very small energy gaps between them, such as 0.204 keV (between Eu L_α and Gd L_α), 0.22 keV (Tb L_α and Dy L_α), 0.148 keV (Gd L_α and Sm L_β), 0.072 keV (Tb L_α and Sm L_β), 0.129 keV (Lu L_α and Ho L_β), etc. Spectrum fitting using the AXIL-based program is not sufficient when the energy gap between the lines is closer to or lower than the inherent resolution of the detector used. Hence, we independently determined the concentrations of lanthanides using this algorithm and compared the results with the PLSR-based algorithm, as shown in Table T4 (SI). Except for two lanthanides (Eu and

https://doi.org/10.1021/acsomega.3c05139
ACS Omega 2023, 8, 41402−41410

Tm), the AXIL-based program was found to provide concentration values with >10−30% positive or negative bias.

3.3. Partial Least-Squares Regression Analysis. The simultaneous determination of ten lanthanides by TXRF spectrometry required multivariate calibration due to the severe spectral overlapping of L lines, as evident from Figure 3. The emission spectrum ranging from the 4 to 11 keV region, which constitutes the complex overlapping L lines of all of the lanthanides, was used for PLSR analysis.

3.3.1. Optimization of the Number of Factors. The number of factors that must be incorporated into the algorithm for creating the model in the PLSR calibration technique had a significant effect on the accuracy and precision of the model that was produced. Because the factors are the redistributed version of the overall variance, using more than the required factors in the model generation may introduce excessive noise, leading to overfitting of calibration data. The number of factors in this study was optimized by calculating the prediction error sum of squares (PRESS) value using the "leave-one-out" approach.[44] Figure S6 (SI) depicts the change in PRESS as a function of the number of components in the model. In Figure S6, the factor number corresponding to the lowest PRESS value reveals the ideal factor numbers for error reduction for the various elements. The factor(min) values were 6, 6, 5, 5, 5, 4, 4, 4, 4, and 4 for La, Nd, Sm, Eu, Gd, Tb, Dy, Ho, Tm, and Lu, respectively. Figure S6 further shows that when factor-(min) is achieved, the PRESS value remains practically constant or slightly increases in certain situations, suggesting the inclusion of noise information into the PLSR model with increasing factor numbers. Because the factor (min) values were so comparable, a default value of 5 was applied for all ten lanthanides.

3.3.2. PLSR Coefficient. Once the number of factors had been optimized, the PLSR coefficient (i.e., PLSRC), which relates the importance of individual variables or energies with element concentration, was constructed. This gave the idea of which parts of spectra had been majorly involved in the correlation of concentration with spectra. Graphical representations of PLSRC for individual lanthanides are shown in Figures S7−S16 (SI). The topmost plots in these figures (Figures S7−S16) show the TXRF spectra of a randomly chosen sample in the 4−11 keV region. In the bottom three figures, the PLSRC is plotted against the energy. The first three factors clearly show a positive coefficient for lanthanide X-ray lines, for which the model was created. Due to the overlapping nature of other lanthanide lines, the negative coefficient is being generated. Sometimes, little energy can accidentally get a positive correlation, e.g., 7.67 and 8.76 keV in Ln's PLSRC factor 1. However, in factor 4 or 6, they are completely absent. This also indicates the requirement for factor optimization to avoid accidental matching. Figure 4 shows the comparison of factor 5 for all of the ten lanthanides with the highest positive coefficient indicated. These highest positive coefficient peaks merge at the exact energy corresponding to the individual TXRF emission. The exact matching of the coefficient peak with the individual L lines of the lanthanides clearly demonstrates the mathematical reason behind the superior analysis power of multivariate analysis mode in a complex overlapping spectral situation. Energies with positive coefficients may occasionally contain contributions from other elements due to the high degree of the overlap spectrum. This could result in an overestimation of the concentration of the relevant element. This overestimation is automatically

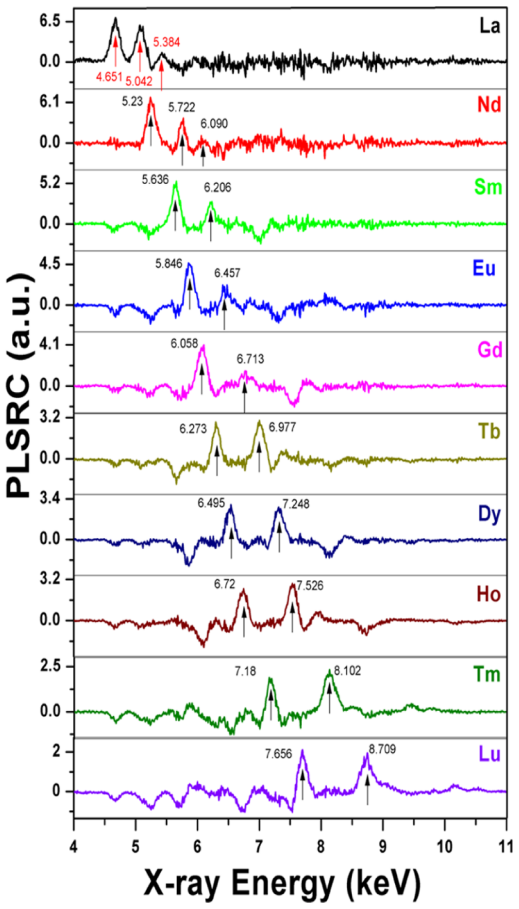

Figure 4. PLSRC for all ten lanthanides obtained for factor 5. The coefficient peak value exactly matches the respective L lines of the particular lanthanide.

corrected by the PLSR algorithm by introducing a negative coefficient at the appropriate energy. For instance, the 5.23 keV Nd-L_α line spectrally overlaps the 5.042 keV La-L_β line. The positive coefficient for La-L_β at 5.042 keV is therefore overestimated. As a result, La has a negative coefficient at 5.23 keV.

3.3.3. Accuracy and Precision. The prognostic ability of the PLSR method was validated by determining the %bias (i.e., accuracy) and %RSD (i.e., precision) for all of the ten lanthanides in the full dynamic range of 0.25−5.25 mg L^{-1} (see Table T1, SI) using the leave-one-out approach. In the CPE process, the selected lanthanides were preconcentrated from a 40 mL aliquot to 0.2 mL of SRP. As a result, the elements get preconcentrated 200 times experimentally, and this factor is different from the preconcentration factor discussed above. Hence, the five VS standard mixtures used in the study were diluted 200 times to carry out the CPE process, followed by TXRF and PLSR analyses. Figure S17 (SI) shows the obtained accuracy and precision for all individual lanthanides in different concentrations. It was interesting to note that, for all of the lanthanides with concentrations ≥2 mg L^{-1}, an accuracy precision of ≤10% was achieved. For the ≤2 mg L^{-1} region, a poor prediction result was obtained. This poor performance in the ≤2 mg L^{-1} region is probably due to a higher error in the PLSRC, which is a common phenomenon in the low-concentration region of the calibration dynamic range. The recovery results for the $Ln_{VS}16$ validation set sample in Table T4 (SI) by both AXIL and PLSR algorithms validated the need

https://doi.org/10.1021/acsomega.3c05139
ACS Omega 2023, 8, 41402−41410

for the latter. Except for Ho, which had a very low concentration of 0.25 mg L^{-1}, the recovery results for the rest of the lanthanides were obtained with an accuracy precision of <10%. Even though the results for Tm and Lu were satisfactory at a concentration level of 1.25 mg L^{-1}, the results for such concentration level deviate much, as shown in Figure S17 (SI). Hence, a minimum of 2 mg L^{-1} lanthanide concentration, which corresponds to 10 μg L^{-1} in the actual sample before preconcentration (due to 200 times dilution), was set as the quantification limit (QL). Therefore, the proposed analytical procedure would be applicable to the sample solutions having the selected ten lanthanides in the range from 10 to 5.25 × 10^3 μg L^{-1}.

3.4. Effect of Common Interfering Ions. Environmental samples always accompany a large amount of commonly occurring elements along with the element(s) of interest. These elements can affect the quantitative extraction of lanthanides and interfere with the L lines of the lanthanides. Hence, we have analyzed the $Ln_{CS}5$ sample from Table T1 in the presence of different concentrations of the interfering ions. The large abundance of alkali metals in nature may affect the clouding behavior without even getting extracted. On the other hand, alkaline earth metals and transition elements may get extracted along with the analytes of interest due to their higher oxidation states. Ethylenediamine tetraacetic acid (EDTA; 0.1 mol L^{-1}) was used as a masking agent to eliminate the interference from Cr^{3+} and Fe^{3+} ions. The effects of some commonly occurring anions were also studied. The tolerance levels of different interfering cations and anions were achieved when their presence did not lower the %Rec of all ten lanthanides below 95%. The results of the interference studies are given in Table 1.

Table 1. Interference Studies of the Method to Commonly Available Cations and Anions[a]

metal ion ($M^{n\pm}$)[b]	tolerance limit (mg L^{-1})
Na^+, K^+	2000
Li^+	1000
Ca^{2+}	500
Mg^{2+}, Sr^{2+}, Ba^{2+}	250
Al^{3+}	100
Cr^{3+}, Fe^{3+}	50[c]
Mn^{2+}, Co^{2+}	200
Pb^{2+}, Hg^{2+}	100
UO_2^{2+}, Th^{4+}	10
Cl^-, Br^-	2000
CO_3^{2-}, PO_4^{3-}, SO_4^{2-}	1000

[a]Experiments were carried out with the LnCS5 solution. [b]Cations were prepared by using their chloride or nitrate salts. Anions were prepared by using their sodium or potassium salts. [c]Determined in the presence of 0.1 mol L^{-1} EDTA.

3.5. Analytical Figures of Merit. The closeness among the L_α lines of the lanthanide series of elements makes their simultaneous determination difficult by XRF spectroscopy. In addition, the nonuniformed concentrations of various lanthanides in environmental samples may cause severe spectral overlapping and make the spectrum more complex. To the best of authors' knowledge, to date, no reports are available on the ultratrace level quantification of such a large number of lanthanides (ten in our case) by TXRF spectroscopy. A comparative study of ultratrace level determination of lanthanides by TXRF spectroscopy is given in Table T5 (SI). It can be seen that a maximum of three to four lanthanides whose L_α lines are well apart were quantified in most of the studies at the ultratrace level.[4,45] In some other literature reports, up to seven lanthanides were determined but at higher concentrations.[17,18,46] In 2017, Oskolok et al.[47] reported the simultaneous determination of five light lanthanides at the 0.04−0.05 μg L^{-1} level using liquid−liquid microextraction-assisted TXRF spectroscopy. Their sample preparation involved dual precipitation, filtration, evaporation, microfiltration, microinsertion, etc., which is much more cumbersome compared to our CPE technique. The large sample volume (500 mL), small preconcentrated volume (100 μL), high amount of deposition (5 drops by 10 μL), and longer acquisition time (1000 s) enabled them to report such improved quantification limit (QL) values. However, in absolute weight terms, their method was capable of analyzing a minimum of 10 ng of a lanthanide, which is not very different from our absolute QL value of 20 ng. Their work is limited to five light lanthanides only, whereas we had simultaneously determined ten lanthanides considering light, middle, and heavy ones. The multivariate calibration curves originating from the PLSR algorithm of TXRF spectra were found to be linear in the range from 10 to 5 × 10^3 μg L^{-1}. The PF values for all of the ten lanthanides were found to be in the range of 124−133. Since the preconcentration processes mentioned in Table T5 (SI) are different from each other, there is no point in comparing their PF values. The CPE of lanthanides by TODGA provided a high degree of selectivity in the presence of a large amount of common interfering ions, which was missing in the previous reports. Other than TXRF spectroscopy, Saito et al.[48] carried out simultaneous preconcentration of 14 lanthanide elements using capillary electrophoresis. Based on the mitigation time, they were able to separate the lanthanides except Sm, Eu, and Gd. Moreover, the methodology was applied for the separation of lanthanides having 50 μM concentration, which is equivalent to 7−9 mg L^{-1} elemental concentration depending on the element analysis. However, in our work, we analyzed highly interfering lanthanide elements, including Sm, Eu, and Gd, down to 10 μg L^{-1}.

3.6. Analysis of Real Samples. The proposed analytical procedure was applied to three CRMs spiked with the ten lanthanides of interest. Rather than applying the methodology to synthetic samples prepared by spike addition, the analyses of CRMs offered much more confidence in method validation. The CRMs used were NASS-7 seawater, SLRS-6 river water, and NIST 1640a natural water, along with added lanthanide concentrations. The added and recovered lanthanide concentrations are tabulated in Table 2. All ten lanthanides were recovered by >98%, and the RSDs were ≤10%.

4. CONCLUSIONS

The potential of using the XRF technique for determining ultratrace quantities of ten lanthanides with low fluorescence yields and overlapping L_α lines had been demonstrated. The offline conjunction of TODGA-assisted CPE with the TXRF technique eliminated the problem of low fluorescence yields by preconcentration. On the other hand, the PLSR algorithm deconvoluted the overlapping spectra. The presence of TODGA and RTIL in the TTX-114 micelles offered high extractability and selectivity toward the lanthanides at pH 4. A large number of commonly available cations and anions were

https://doi.org/10.1021/acsomega.3c05139
ACS Omega 2023, 8, 41402−41410

Table 2. Analysis of Real Samples ($N = 5$)[a]

	NASS-7 seawater[b]		SLRS-6 river water[b]		NIST 1640a natural water[c]	
element	added ($\mu g\ L^{-1}$)	found ($\mu g\ L^{-1}$)	added ($\mu g\ L^{-1}$)	found ($\mu g\ L^{-1}$)	added ($\mu g\ L^{-1}$)	found ($\mu g\ L^{-1}$)
La	13	12.8 ± 1.0 (98.5)	18	17.8 ± 1.3 (98.9)	38	37.4 ± 1.6 (98.4)
Nd	18	17.7 ± 1.3 (98.3)	26	25.6 ± 1.7 (98.5)	32	31.6 ± 1.6 (98.8)
Sm	22	21.8 ± 1.3 (99.2)	14	13.8 ± 1.2 (98.6)	40	39.3 ± 1.7 (98.3)
Eu	15	14.9 ± 1.6 (99.3)	35	34.7 ± 1.7 (99.1)	21	20.7 ± 1.4 (98.6)
Gd	28	27.6 ± 1.7 (98.6)	20	19.7 ± 1.4 (98.5)	25	24.7 ± 1.5 (98.8)
Tb	25	24.7 ± 1.4 (98.8)	22	21.6 ± 1.3 (98.2)	28	27.6 ± 1.7 (98.6)
Dy	20	19.8 ± 1.4 (99)	33	32.7 ± 1.8 (99.2)	45	44.2 ± 1.5 (98.2)
Ho	32	31.5 ± 1.6 (98.4)	15	14.8 ± 1.1 (98.7)	23	22.8 ± 1.4 (99.1)
Tm	24	23.7 ± 1.4 (98.8)	17	16.7 ± 1.2 (98.2)	50	49.2 ± 1.5 (98.4)
Lu	19	18.7 ± 1.5 (98.4)	30	29.6 ± 1.5 (98.7)	26	25.8 ± 1.6 (99.2)

[a]Note: the percentage recoveries are given in parentheses. [b]The certified lanthanide concentrations are more than 1500 times less than the QL of our method. [c]No certified lanthanide concentrations are mentioned for these CRMs.

found to have no effect on the preconcentration process. The PLSR analyses of the recorded TXRF spectra resulted in a PLSR coefficient for an individual element. As a result, all of the ten lanthanides can be determined in the range from 10 to $5 \times 10^3\ \mu g\ L^{-1}$. To the best of authors' knowledge, to date, no reports claim such low-level determination of ten lanthanides simultaneously by the XRF technique.

■ ASSOCIATED CONTENT

Supporting Information

The Supporting Information is available free of charge at https://pubs.acs.org/doi/10.1021/acsomega.3c05139.

Brief introduction about the PLSR algorithm, schematic of cloud point-based extraction of lanthanides, effect of TODGA and TTX-114 concentration on the recovery of ten lanthanides, effect of temperature on the average size of micelles, effect of phase separation temperature on the preconcentration factor, evolution of PRES, PLSRC data, and %bias and %RSD for all ten lanthanides (PDF)

■ AUTHOR INFORMATION

Corresponding Authors

Abhijit Saha − *Radioanalytical Chemistry Division, Bhabha Atomic Research Centre, Mumbai 400085, India;* orcid.org/0000-0002-5034-080X; Email: abhi.gallary@gmail.com

Arnab Sarkar − *Fuel Chemistry Division, Bhabha Atomic Research Centre, Mumbai 400085, India; Homi Bhabha National Institute, Mumbai 400094, India;* orcid.org/0000-0003-3783-8299; Email: arnab@barc.gov.in

Authors

Kaushik Sanyal − *Fuel Chemistry Division, Bhabha Atomic Research Centre, Mumbai 400085, India; Homi Bhabha National Institute, Mumbai 400094, India;* orcid.org/0000-0001-5964-970X

Sadhan Bijoy Deb − *Radioanalytical Chemistry Division, Bhabha Atomic Research Centre, Mumbai 400085, India*

Rajesh V. Pai − *Fuel Chemistry Division, Bhabha Atomic Research Centre, Mumbai 400085, India; Homi Bhabha National Institute, Mumbai 400094, India;* orcid.org/0000-0002-9258-2751

Manoj Kumar Saxena − *Radioanalytical Chemistry Division, Bhabha Atomic Research Centre, Mumbai 400085, India;* orcid.org/0000-0002-9997-4328

Complete contact information is available at: https://pubs.acs.org/10.1021/acsomega.3c05139

Notes

The authors declare no competing financial interest.

■ ACKNOWLEDGMENTS

The authors are thankful to Dr. P.K. Mohapatra, Associate Director RC & IG, BARC, for his constant encouragement.

■ REFERENCES

(1) Rao, T. P.; Biju, V. Trace Determination of Lanthanides in Metallurgical, Environmental, and Geological Samples. *Crit. Rev. Anal. Chem.* **2000**, *30* (2−3), 179−220.

(2) Ornatsky, O. I.; Kinach, R.; Bandura, D. R.; Lou, X.; Tanner, S. D.; Baranov, V. I.; Nitz, M.; Winnik, M. A. Development of analytical methods for multiplex bio-assay with inductively coupled plasma mass spectrometry. *J. Anal. At. Spectrom.* **2008**, *23* (4), 463−469.

(3) Miaokang, S.; Yinyu, S. Determination of lanthanum, europium, and ytterbium in food samples by electrothermal atomic absorption spectrometry. *J. AOAC Int.* **1992**, *75* (4), 667−671.

(4) Sá, Í. P.; Almeida, O. N.; Lima, D. D. C.; da Silva, E. G.; Santos, L. N.; Luzardo, F. H.; Velasco, F. G.; Gonzalez, M. H.; Amorim, F. A. Determination of lanthanide and actinide elements by energy dispersive x-ray fluorescence spectrometry applying DLLME preconcentration and dried spot. *Spectrochim. Acta, Part B* **2021**, *182*, No. 106253.

(5) Kulaksız, S.; Bau, M. Rare earth elements in the Rhine River, Germany: First case of anthropogenic lanthanum as a dissolved microcontaminant in the hydrosphere. *Environ. Int.* **2011**, *37* (5), 973−979.

(6) Anawar, H. M.; Freitas, M. d.; Canha, N.; Dionísio, I.; Dung, H.; Galinha, C.; Pacheco, A. Assessment of bioaccumulation of REEs by plant species in a mining area by INAA. *J. Radioanal. Nucl. Chem.* **2012**, *294* (3), 377−381.

(7) Pagano, G.; Guida, M.; Tommasi, F.; Oral, R. Health effects and toxicity mechanisms of rare earth elements-Knowledge gaps and research prospects. *Ecotoxicol. Environ. Saf.* **2015**, *115*, 40−48.

(8) Cheng, J.; Li, N.; Cai, J.; Cheng, Z.; Hu, R.; Zhang, Q.; Wan, F.; Sun, Q.; Gui, S.; Sang, X.; et al. Organ histopathological changes and its function damage in mice following long-term exposure to lanthanides chloride. *Biol. Trace Elem. Res.* **2012**, *145* (3), 361−368.

(9) Blinova, I.; Lukjanova, A.; Muna, M.; Vija, H.; Kahru, A. Evaluation of the potential hazard of lanthanides to freshwater microcrustaceans. *Sci. Total Environ.* **2018**, *642*, 1100−1107.

(10) Weltje, L.; Verhoof, L. R.; Verweij, W.; Hamers, T. Lutetium speciation and toxicity in a microbial bioassay: testing the free-ion model for lanthanides. *Environ. Sci. Technol.* **2004**, *38* (24), 6597−6604.

(11) Pałasz, A.; Czekaj, P. Toxicological and cytophysiological aspects of lanthanides action. *Acta Biochim. Polym.* **2000**, *47* (4), 1107−1114.
(12) Balaram, V. Rare earth elements: A review of applications, occurrence, exploration, analysis, recycling, and environmental impact. *Geosci. Front.* **2019**, *10* (4), 1285−1303.
(13) Bertin, E. P. *Introduction to X-ray Spectrometric Analysis*; Springer Science & Business Media: New York, 2013.
(14) Sanyal, K.; Kanrar, B.; Dhara, S.; Misra, N.; Wobrauschek, P.; Streli, C. Results from a new low Z -high Z TXRF Spectrometer. *Adv. X-Ray Anal.* **2016**, *59*, 125−143.
(15) Klockenkämper, R. Total Reflection X-Ray Fluorescence Analysis. In *Chemical Analysis*; John Wiley: New York, 1997; Vol. *140*.
(16) Klockenkämper, R.; Bohlen, A. V. Worldwide distribution of total reflection X-ray fluorescence instrumentation and its different fields of application: A survey. *Spectrochim. Acta, Part B* **2014**, *99*, 133−137.
(17) Orescanin, V.; Mikelic, L.; Roje, V.; Lulic, S. Determination of lanthanides by source excited energy dispersive X-ray fluorescence (EDXRF) method after preconcentration with ammonium pyrrolidine dithiocarbamate (APDC). *Anal. Chim. Acta* **2006**, *570* (2), 277−282.
(18) Kirsanov, D.; Panchuk, V.; Goydenko, A.; Khaydukova, M.; Semenov, V.; Legin, A. Improving precision of X-ray fluorescence analysis of lanthanide mixtures using partial least squares regression. *Spectrochim. Acta, Part B* **2015**, *113*, 126−131.
(19) Meira, L. A.; Almeida, J. S.; Dias, F. d. S.; Pedra, P. P.; Pereira, A. L. C.; Teixeira, L. S. Multi-element determination of Cd, Pb, Cu, V, Cr, and Mn in ethanol fuel samples using energy dispersive X-ray fluorescence spectrometry after magnetic solid phase microextraction using $CoFe_2O_4$ nanoparticles. *Microchem. J.* **2018**, *142*, 144−151.
(20) Saha, A.; Sanyal, K.; Rawat, N.; Deb, S. B.; Saxena, M. K.; Tomar, B. S. Selective micellar extraction of ultratrace levels of uranium in aqueous samples by task specific ionic liquid followed by its detection employing total reflection X-ray fluorescence spectrometry. *Anal. Chem.* **2017**, *89* (19), 10422−10430.
(21) Favre-Réguillon, A.; Draye, M.; Lebuzit, G.; Thomas, S.; Foos, J.; Cote, G.; Guy, A. Cloud point extraction: an alternative to traditional liquid−liquid extraction for lanthanides(III) separation. *Talanta* **2004**, *63* (3), 803−806.
(22) Bahadir, Z.; Torrent, L.; Hidalgo, M.; Margui, E. Simultaneous determination of silver and gold nanoparticles by cloud point extraction and total reflection X-ray fluorescence analysis. *Sens. Actuators, B* **2018**, *149*, 22−29.
(23) Saha, A.; Debnath, T.; Neogy, S.; Ghosh, H. N.; Saxena, M. K.; Tomar, B. S. Micellar extraction assisted fluorometric determination of ultratrace amount of uranium in aqueous samples by novel diglycolamide-capped quantum dot nanosensor. *Sens. Actuators, B* **2017**, *253*, 592−602.
(24) De Jong, N.; Draye, M.; Favre-Réguillon, A.; LeBuzit, G.; Cote, G.; Foos, J. Lanthanum(III) and gadolinium(III) separation by cloud point extraction. *J. Colloid Interface Sci.* **2005**, *291* (1), 303−306.
(25) Mustafina, A.; Elistratova, J.; Burilov, A.; Knyazeva, I.; Zairov, R.; Amirov, R.; Solovieva, S.; Konovalov, A. Cloud point extraction of lanthanide(III) ions via use of Triton X-100 without and with water-soluble calixarenes as added chelating agents. *Talanta* **2006**, *68* (5), 863−868.
(26) Saha, A.; Deb, S. B.; Sarkar, A.; Saxena, M. K.; Tomar, B. S. Simultaneous preconcentration of uranium and thorium in aqueous samples using cloud point extraction. *RSC Adv.* **2016**, *6* (24), 20109−20119.
(27) Vekemans, B.; Janssens, K.; Vincze, L.; Adams, F.; Espen, P. V. Comparison of several background compensation methods useful for evaluation of energy-dispersive X-ray fluorescence spectra. *Spectrochim. Acta, Part B* **1995**, *50* (2), 149−169.
(28) Depoi, F. d. S.; Bentlin, F. R. S.; Ferrão, M. F.; Pozebon, D. Multivariate optimization for cloud point extraction and determination of lanthanides. *Anal. Methods* **2012**, *4*, 2809−2814.
(29) dos Santos, F. R.; de Oliveira, J. F.; Bona, E.; Barbosa, G. M.; Melquiades, F. L. Evaluation of pre-processing and variable selection on energy dispersive X-ray fluorescence spectral data with partial least square regression: A case of study for soil organic carbon prediction. *Spectrochim. Acta, Part B* **2021**, *175*, No. 106016.
(30) Dicholkar, D. D.; Kumar, P.; Heer, P. K.; Gaikar, V. G.; Kumar, S.; Natarajan, R. Synthesis of N,N,N′,N′-tetraoctyl-3-oxapentane-1,5-diamide (TODGA) and its steam thermolysis-nitrolysis as a nuclear waste solvent minimization method. *Ind. Eng. Chem. Res.* **2013**, *52*, 2457−2469.
(31) Sanyal, K.; Kanrar, B.; Mishra, N. L.; Czyzycki, M.; Migliori, A.; Karydas, A. G. A comparative study on the total reflection X-ray fluorescence determination of low Z elements using X-ray tube and synchrotron radiation as excitation sources. *X-Ray Spectrom.* **2017**, *46*, 164−170.
(32) Wobrauschek, P. Total reflection x-ray fluorescence analysis—a review. *X-Ray Spectrom.* **2007**, *36*, 289−300.
(33) Wobrauschek, P.; Prost, J.; Ingerie, D.; Kregsamer, P.; Mishra, N. L. C. A novel vacuum spectrometer for total reflection x-ray fluorescence analysis with two exchangeable low power x-ray sources for the analysis of low, medium, and high Z elements in sequence. *Rev. Sci. Instrum.* **2015**, *86*, No. 083105.
(34) Chan, G.C.-Y.; Mao, X.; Choi, I.; Sarkar, A.; Lam, O. P.; Shuh, D. K.; Russo, R. E. Multiple emission line analysis for improved isotopic determination of uranium—a computer simulation study. *Spectrochim. Acta, Part B* **2013**, *89*, 40−49.
(35) Sarkar, A.; Mao, X.; Chan, G. C. Y.; Russo, R. E. Laser ablation molecular isotopic spectrometry of water for $_1D^2/_1H^1$ ratio analysis. *Spectrochim. Acta, Part B* **2013**, *88*, 46−53.
(36) Sarkar, A.; Mao, X.; Russo, R. E. Advancing the analytical capabilities of laser ablation molecular isotopic spectrometry for boron isotopic analysis. *Spectrochim. Acta, Part B* **2014**, *92*, 42−50.
(37) Labrecque, C.; Potvin, S.; Whitty-Léveillé, L.; Larivière, D. Cloud point extraction of uranium using H_2DEH[MDP] in acidic conditions. *Talanta* **2013**, *107*, 284−291.
(38) Shimojo, K.; Kurahashi, K.; Niganawa, H. Extraction behavior of lanthanides using a diglycolamide derivative TODGA in ionic liquids. *Dalton Trans.* **2008**, *37*, 5083−5088.
(39) Husain, M.; Ansari, S. A.; Mohapatra, P. K.; Gupta, R. K.; Parmar, V. S.; Manchanda, V. K. Extraction chromatography of lanthanides using N,N,N′,N′-tetraoctyl diglycolamide (TODGA) as the stationary phase. *Desalination* **2008**, *229*, 294−301.
(40) Vekemans, B.; Janssens, K.; Vincze, L.; Adams, F.; Van Espen, P. Analysis of X-ray spectra by iterative least squares (AXIL): New developments. *X-Ray Spectrom.* **1994**, *23* (6), 278−285.
(41) Solé, V.; Papillon, E.; Cotte, M.; Walter, P.; Susini, J. A multiplatform code for the analysis of energy-dispersive X-ray fluorescence spectra. *Spectrochim. Acta, Part B* **2007**, *62* (1), 63−68.
(42) Sanyal, K.; Dhara, S. Direct non-destructive trace and major elemental analysis in steel samples utilizing micro-focused brems-strahlung radiation in X-ray fluorescence geometry. *Anal. Sci.* **2022**, *38*, 665−673.
(43) Sanyal, K.; Dhara, S.; Sanjay Kumar, S.; Mishra, N. L.; Mollick, P. K.; Rao, P. T.; Venugopalan, R.; Pai, R. V.; Kumar, N.; Mukherjee, S. K.; Chakravartty, J. K.; Aggarwal, S. K. Application of TXRF for burn leach test of TRISO coated UO_2 particles. *J. Radioanal. Nucl. Chem.* **2014**, *302*, 1357−1361.
(44) Xu, S. Predicted residual error sum of squares of mixed models: An application for genomic prediction. *G3: Genes Genomes Genet.* **2017**, *7* (3), 895−909.
(45) De Vito, I. E.; Olsina, R. A.; Masi, A. N. Enrichment method for trace amounts of rare earth elements using chemofiltration and XRF determination. *Fresenius' J. Anal. Chem.* **2000**, *368*, 392−396.
(46) D'Angelo, J. A.; Martinez, L. D.; Resnizky, S.; Perino, E.; Marchevsky, E. J. Determination of eight lanthanides in apatites by ICP-AES, XRF, and NAA. *J. Trace Microprobe Tech.* **2001**, *19*, 79−90.
(47) Oskolok, K. V.; Monogarova, O. V.; Alov, N. V. Total reflection X-ray fluorescence determination of rare earth elements in mineral water using a combined preconcentration technique. *Anal. Lett.* **2017**, *50*, 2900−2907.

https://doi.org/10.1021/acsomega.3c05139
ACS Omega 2023, 8, 41402−41410

(48) Saito, S.; Hoshino, H. Highly-sensitive simultaneous detection of lanthanide(III) ions as kinetically stable aromatic polyaminocarboxylato complexes via capillary electrophoresis using resolution enhancement with carbonate ion. *Anal. Bioanal. Chem.* **2004**, *378*, 1644−1647.

https://doi.org/10.1021/acsomega.3c05139
ACS Omega 2023, 8, 41402−41410